Description of a Proposed On-Orbit Calibration Procedure for SIM Based On Spacecraft Maneuver

Miltiadis V. Papalexandris, Mark H. Milman, and Stuart Shaklan

Jet Propulsion Laboratory,
California Institute of Technology,
Pasadena, CA 91109

ABSTRACT

The astrometric performance of the Space Interferometry Mission (SIM) relies on precise measurements of the optical pathlength difference of the starlight through the arms of the interferometers that comprise the SIM instrument, and on precise relative distance between a set of fiducials that define the baselines of the interferometers. The accuracy of these measurements can be affected by various phenomena. Some of them are time-dependent (e.g., time-varying temperatures of components), while others are relatively static and repeatable (e.g., diffraction and polarization effects due to controlled translations and rotations of components). In this work we are concerned with the instrument errors of the latter type and in their compensation. In particular, a procedure for on-orbit calibration of the instrument error function is defined, and a proof of concept of its viability is presented. On a given grid of stars, the proposed procedure generates approximations of the gradient of the instrument error function at a discrete set of field points corresponding to the star locations via a specialized set of maneuvers of the spacecraft. These gradient approximations are then used to estimate the error function via a least squares procedure in a manner that is very analogous to the wavefront reconstruction problem in adaptive optics systems. An error analysis of the procedure is presented providing further insights into the connections between instrument errors and the grid reduction solution. Finally, numerical results are presented on a randomly generated grid of stars that demonstrate the feasibility of the method.

Keywords: Space Interferometry Mission, On-Orbit Calibration, least-squares optimization.

1. INTRODUCTION

The Space Interferometry Mission (SIM) derives its performance from precise (relative) distance measurements made between a set of fiducials. The accuracy of these measurements can degrade from a number of reasons. Some of them are time-dependent (e.g., time-varying temperatures of various components), while others are relatively static and repeatable (e.g., diffraction effects due to delay-line motion, polarization effects due to cornercube rotations etc). In this memo we are concerned with the errors of the latter type, that is, errors that can essentially be parameterized by the position of an object in the instrument's field of regard.

The magnitude of these errors can be very large, up to 20 nm over the field of regard for the science interferometer. On the other hand, the measurements of the instrument must be accurate to a level of approximately 0.5 nm. Consequently, highly accurate calibration procedures for the instrument's delay measurements are necessary. Fortunately, these error sources have to be calibrated for the science interferometer only and not for the guide interferometers, since over an observation period the positions of the guide stars are stationary with respect to the field of regard. The calibration procedure must satisfy tight accuracy requirements as well as duration requirements. Since calibration will be performed on orbit, it is desirable to be completed as quickly as possible in order to maximize the time that is available for science measurements, and to minimize errors due to time–varying effects.

In this memo, a procedure for "external" calibration is presented. By "external" we mean that the instrument is calibrated using inertial sources. The basic measurement of the instrument is the delay measurement, d, given by

$$d = < \boldsymbol{s}, \boldsymbol{b} > + c(\boldsymbol{s}, \boldsymbol{b}), \tag{1}$$

where $< \cdot, \cdot >$ denotes the usual Euclidian inner product of two vectors in E^3, $\boldsymbol{s}$ is a science star vector, $\boldsymbol{b}$ is the baseline vector of the interferometer, and $c(\boldsymbol{s}, \boldsymbol{b})$ is the calibration function.

The objective of this work is to calculate c. If the vectors $\boldsymbol{b}$ and $\boldsymbol{s}$ were known precisely, then a single measurement of the instrument would suffice to compute the value of c at the field location directly from (1). This computation would be subject only to the measurement (shot) noise of the instrument. However, neither $\boldsymbol{b}$ nor $\boldsymbol{s}$ are known precisely. For example, the star positions, $\boldsymbol{s}$, may be known only to several *mas*, while the error in the measurement of the baseline length, $|\boldsymbol{b}|$ can be on the order of a few μm. The combined effect of the uncertainties in d, $\boldsymbol{s}$, and $\boldsymbol{b}$ is such that direct use of (1) for the calculation of the calibration function c results in errors that are orders of magnitude greater than the required precision, [3]. It is, therefore, required to explore other methodologies for external calibration of the interferometer.

Although c is practically unobservable by direct examination of (1), it turns out that more success can be achieved by approximating the *gradient* of c, ∇c. This is accomplished by canting and rolling the instrument by small angles and taking difference measurements. This approach exploits the inherent strengths of the instrument to make precise differential delay measurements. ∇c can thus be computed at any field location occupied by a bright enough star. From these gradients the calibration function is then estimated using a least squares inversion, in a manner very much analogous to wavefront reconstruction methods in adaptive optics.

The error analysis presented here is slightly complicated. We first characterize the "random" noise effects of delay measurement error and star position error. This analysis is relatively straightforward, and the errors are shown to be quite benign. Star position errors of 2–3mas are very tolerable. We also consider the possibility that the star position errors are correlated. This correlation is to be expected if SIM has to "self–start" as a result of not having first performed a dedicated survey of a patch of sky on which to do calibration (e.g., if there is no reliance on precurson mission or a ground survey). Numerical simulations indicate that there is very little degradation in this "self–start" scenario.

Another source of error is the discretization error due to the approximation of ∇c by finite differences developed from delay measurements, and the subsequent reconstruction of c on the finite grid of stars. Relationships between the number of calibration stars, cant/roll angle, measurement noise, and discretization error in the calibration function are developed. The important result here is that noise propagation is reduced by larger cant/roll angles and more calibration stars; however this has to balanced against increasing the discretization error and time required for performing the calibration. The correct balance is strongly dependent on the nature of the calibration function itself, and as (if) external calibration proceeds, characterizing the calibration function in a manner to make this determination will be an on–going investigation in the testbeds. (Some ideas on this process are also included.)

The remaining source of error considered in this memo is due to inaccurate knowledge of the baseline vector. An analysis of the least squares solution reveals that the major resulting error in the estimation of the calibration function is essentially *linear* across the field. This is signficant because a linear error in the calibration function is indistinguishable from a change in the baseline vector, and consequently has no impact on the determination of the astrometric parameters of the stars. This notion that linear errors across the field are inconsequential to performing astrometry is a potential linchpin idea that will probably be exploited in many ways.

The following sections contain the details of the calibration scheme along with the derivation of specific formulae and bounds for the effects of the various error sources. Numerical results that demonstrate the efficacy of the method are also included.

2. ON-ORBIT CALIBRATION SCHEME

The proposed method for such a task relies on setting up a grid of stars and canting and rolling of the intrument by small angles (at the order of 1°) and use of (1) to obtain estimates of the spatial derivatives of c at the grid points. Setting these estimates equal to the corresponding finite-difference approximations of the spatial derivatives of c results in an overdetermined linear system that can be solved in a least-squares sense to compute the values of c at the grid points. Once this is achieved, the value of c at any other point inside the grid can be computed by means of two-dimensional interpolation.

To fix ideas, let D denote a region in the $u-v$ plane containing the origin. A point in D is denoted by $\boldsymbol{x} = (u, v)$. Further, let S denote the unit sphere, and define the mapping $\boldsymbol{s} : D \to S$ by

$$\boldsymbol{s}(u,v) \;=\; (u, v, \gamma(u,v)), \quad \gamma(u,v) = \sqrt{1-(u^2+v^2)}\,. \tag{2}$$

In other words, $\boldsymbol{s}$ provides a parametrization of the instrument's field of regard. A typical size of a circular field of regard is 15°, for which we have $u^2 + v^2 \leq (7.5\pi/180)^2$. According to this parametrization, the center of the field of regard is $(0, 0, 1)$. The proposed calibration scheme consists of the following steps.

Step 1. Select a coordinate system so that the baseline vector $\boldsymbol{b}$ is colinear to $(1, 0, 0)$. Then, select a grid $G_S \in S$ consisting of $N \times N$ stars in the field of regard, $G_S = \{\boldsymbol{s}(i,j) = (u(i,j), v(i,j), \gamma(i,j)), \quad i,j = 1,\ldots,N\}$. The vector array $\boldsymbol{s}$ is assumed to be known *a priori* from star catalogues within some (known) error bounds. Further, the mapping $\boldsymbol{s}$ given by (2) defines a grid of points $G_D = \{\boldsymbol{x}(i,j), \quad i,j = 1,\ldots,N\} \in D$ which corresponds to the grid of stars G_S. It is desirable to have as many grid stars as possible, which menas that for accuracy purposes N must be as large as possible. However, the larger N gets, the slower the calibration procedure becomes (mission requirements state that the duration of the procedure cannot exceed a few hours). Further, there is a limit on the amount of "suitable" stars (in terms of, say, luminosity or relative distance) in any given field of regard. Because of these considerations, the range of N is restricted to $10 < N < 20$.

Step 2. Rotate the instrument baseline $-\alpha$ and α degrees about the $v-$ axis (cant). The rotation matrices are given by

$$R_v^{\pm} \;=\; \begin{bmatrix} \cos\alpha & 0 & \mp\sin\alpha \\ 0 & 1 & 0 \\ \pm\sin\alpha & 0 & \cos\alpha \end{bmatrix}, \tag{3}$$

respectively. Make delay measurements $d_u^+(i,j)$ and $d_u^-(i,j)$, $i,j = 1,\ldots,N$, at the grid points, respectively. Then, application of (1) yields the relationship between the delays and the values of the calibration function at the "rotated" grid points $(u^{\pm}, v)$:

$$d_u^{\pm}(i,j) \;=\; < \boldsymbol{s}(i,j), R_v^{\pm}\boldsymbol{b} > + c\left(u^{\pm}(i,j), v(i,j)\right) \quad i,j = 1,\ldots,N\,, \tag{4}$$

where

$$u^{\pm}(i,j) \;=\; u(i,j) \pm \alpha\,. \tag{5}$$

Step 3. Rotate the instrument baseline β and $-\beta$ degrees about the $u-$ axis (roll). The rotation matrices are given by

$$R_u^{\pm} \;=\; \begin{bmatrix} 1 & 0 & 0 \\ 0 & \cos\beta & \mp\sin\beta \\ 0 & \pm\sin\beta & \cos\beta \end{bmatrix}, \tag{6}$$

respectively. Make measurements $d_v^+(i,j)$ and $d_v^-(i,j)$, $i,j = 1,\ldots,N$, at the grid points, respectively. As before, relation (1) yields,

$$d_v^{\pm}(i,j) \;=< \boldsymbol{s}(i,j), R_u^{\pm}\boldsymbol{b} > + c\left(u(i,j), v^{\pm}(i,j)\right) \quad i,j = 1,\ldots,N\,, \tag{7}$$

where

$$v^{\pm}(i,j) \;=\; v(i,j) \pm \beta\,. \tag{8}$$

Step 4. Calculate approximations of the gradient of c at the grid points

$$\nabla c(i,j) \;\equiv\; \left[\frac{\partial c(i,j)}{\partial u}, \frac{\partial c(i,j)}{\partial v}\right], \tag{9}$$

based on the measurements that were taken during the rotations of Steps 2 and 3. In particular, the following approximations hold:

$$\frac{\partial c(i,j)}{\partial u} \;\simeq\; \frac{1}{2\alpha}\left[c\left(u^+(i,j), v(i,j)\right) - c\left(u^-(i,j), v(i,j)\right)\right], \quad i,j = 1,\ldots,N\,, \tag{10}$$

$$\frac{\partial c(i,j)}{\partial v} \;\simeq\; \frac{1}{2\beta}\left[c\left(u(i,j), v^+(i,j)\right) - c\left(u(i,j), v^-(i,j)\right)\right], \quad i,j = 1,\ldots,N\,. \tag{11}$$

In view of (4) and (6), the above relations yield

$$\frac{\partial c(i,j)}{\partial u} \;\simeq\; \frac{1}{2\alpha}\left[d_u^+(i,j) - d_u^-(i,j) - < \boldsymbol{s}(i,j), (R_v^+ - R_v^-)\boldsymbol{b} >\right], \quad i,j = 1,\ldots,N\,, \tag{12}$$

$$\frac{\partial c(i,j)}{\partial v} \;\simeq\; \frac{1}{2\beta}\left[d_v^+(i,j) - d_v^-(i,j) - < \boldsymbol{s}(i,j), (R_u^+ - R_u^-)\boldsymbol{b} >\right], \quad i,j = 1,\ldots,N\,. \tag{13}$$

Step 5. Calculate the centered, finite-difference approximations of the gradient of c at the 'interior' grid points. The approximations satisfy the following relations:

$$c(i+1,j) - c(i-1,j) \;\simeq< \nabla c(i,j), \boldsymbol{x}(i+1,j) - \boldsymbol{x}(i-1,j) >,\; i = 2,..,N-1,\;\; j = 1,..,N, \tag{14}$$

$$c(i,j+1) - c(i,j-1) \;\simeq< \nabla c(i,j), \boldsymbol{x}(i,j+1) - \boldsymbol{x}(i,j-1) >,\; i = 1,..,N,\;\; j = 2,..,N-1. \tag{15}$$

For the grid points that lie on the boundary of the grid, one-sided differences are used:

$$c(2,j) - c(1,j) \;\simeq< \nabla c(1,j),\, \boldsymbol{x}(2,j) - \boldsymbol{x}(1,j) >, \quad j = 1,\ldots,N\,, \tag{16}$$

$$c(i,2) - c(i,1) \;\simeq< \nabla c(i,1),\, \boldsymbol{x}(i,2) - \boldsymbol{x}(i,1) >, \quad i = 1,\ldots,N\,, \tag{17}$$

$$c(N,j) - c(N-1,j) \;\simeq< \nabla c(N,j),\, \boldsymbol{x}(N,j) - \boldsymbol{x}(N-1,j) >, \quad j = 1,\ldots,N\,, \tag{18}$$

$$c(i,N) - c(i,N-1) \;\simeq< \nabla c(i,N),\, \boldsymbol{x}(i,N) - \boldsymbol{x}(i,N-1) >, \quad i = 1,\ldots,N\,. \tag{19}$$

Step 6. Substitute (12)-(13) into the right-hand side of (14)-(19). The result is an overdetermined system

$$A\,\hat{c} \;=\; \boldsymbol{z}\,, \tag{20}$$

which is solved in the least-squares sense. In the above equation $\hat{c}$ is the N^2-array whose elements are the values of the calibration function at the grid points, *i.e*,

$$\hat{c}(i+(j-1)N) \;=\; c(i,j)\,, \qquad i,j=1,\ldots,N\,. \tag{21}$$

Also, $\boldsymbol{z}$ is the $2\times N^2$-array that arises from substitution of the expression for the gradient of the calibration function c, relations (12) and (13), into the right-hand side of (14)-(19). In other words, $\boldsymbol{z}$ can be written as

$$\boldsymbol{z} \;=\; \left[\boldsymbol{z}^I, \boldsymbol{z}^{II}\right]^{\mathrm{T}}\,, \tag{22}$$

where $\boldsymbol{z}^I$ and $\boldsymbol{z}^{II}$ are N^2-arrays given by

$$\left.\begin{aligned} \boldsymbol{z}^I(1+(j-1)N) &= <\nabla c(1,j),\, \boldsymbol{x}(2,j)-\boldsymbol{x}(1,j)>, \\ \boldsymbol{z}^I(i+(j-1)N) &= <\nabla c(i,j),\, \boldsymbol{x}(i+i,j)-\boldsymbol{x}(i-i,j)>, \quad i=2,\ldots,N-1, \\ \boldsymbol{z}^I(N+(j-1)N) &= <\nabla c(N,j),\, \boldsymbol{x}(N,j)-\boldsymbol{x}(N-1,j)>, \end{aligned}\right\} \tag{23}$$

$j=1,\ldots,N$, and

$$\left.\begin{aligned} \boldsymbol{z}^{II}(i) &= <\nabla c(i,1),\, \boldsymbol{x}(i,2)-\boldsymbol{x}(i,1)>, \\ \boldsymbol{z}^{II}(i+(j-1)N) &= <\nabla c(i,j),\, \boldsymbol{x}(i,j+1)-\boldsymbol{x}(i,j-1)>, \quad j=2,\ldots,N-1, \\ \boldsymbol{z}^{II}(N(N-1)+i) &= <\nabla c(i,N),\, \boldsymbol{x}(i,N)-\boldsymbol{x}(i,N-1)>, \end{aligned}\right\} \tag{24}$$

$i=1,\ldots,N$, respectively. The gradients at the right-hand side of the above expressions are given by (12) and (13).

Finally, A is a $2N^2\times N^2$ matrix and consists of the centered finite-difference operators in the u and v directions (one-sided operators have been used on the boundary). In other words, $A=[A_u, A_v]^{\mathrm{T}}$, where A_u and A_v are given by

$$A_u \;=\; \begin{bmatrix} B & 0 & \cdots & 0 \\ 0 & B & \cdots & 0 \\ \vdots & \vdots & \ddots & \vdots \\ 0 & 0 & \cdots & B \end{bmatrix}, \tag{25}$$

and

$$A_v \;=\; \begin{bmatrix} -2I & 2I & 0 & \cdots & 0 & 0 & 0 \\ -I & 0 & I & \cdots & 0 & 0 & 0 \\ \vdots & \vdots & \vdots & \ddots & \vdots & \vdots & \vdots \\ 0 & 0 & 0 & \cdots & -I & 0 & I \\ 0 & 0 & 0 & \cdots & 0 & -2I & 2I \end{bmatrix}, \tag{26}$$

with I being the $N\times N$ identity matrix and B being the following $N\times N$ block diagonal matrix:

$$B \;=\; \begin{bmatrix} -2 & 2 & 0 & \cdots & 0 & 0 & 0 \\ -1 & 0 & 1 & \cdots & 0 & 0 & 0 \\ \vdots & \vdots & \vdots & \ddots & \vdots & \vdots & \vdots \\ 0 & 0 & 0 & \cdots & -1 & 0 & 1 \\ 0 & 0 & 0 & \cdots & 0 & -2 & 2 \end{bmatrix}. \tag{27}$$

The solution to equation (20) is given by

$$\hat{c} \;=\; A^{\dagger} \cdot \boldsymbol{z}\,, \tag{28}$$

where $A^{\dagger}$ is the pseudo-inverse of A. The computation of $A^{\dagger}$ is performed via the Singular Value Decomposition (SVD). Once the values of the calibration function have been computed at the points of the grid stars, an interpolation scheme, *e.g.* linear or parabolic interpolation, can be employed to evaluate the calibration function at other points of the field of regard.

It is worth mentioning that the continuous least-squares problem associated with (18) is to minimize the functional J:

$$J(c) \;=\; \min_{c} \int_{D} |\nabla c(u,v) - \boldsymbol{y}|^2 \, ds\,. \tag{29}$$

The solution to this problem solves the following boundary-value problem on D:

$$\nabla^2 c(u,v) - \nabla \cdot \boldsymbol{y} \;=\; 0\,, \quad (u,v) \in D\,, \tag{30}$$

with Neumann boundary conditions

$$\nabla_n c(u,v) \;=\; \boldsymbol{y}_n\,, \quad (u,v) \in \partial D\,. \tag{31}$$

In the above expressions $\boldsymbol{y}$ is a, presumably known, continuously differentiable function, satisfying $\boldsymbol{y} = (\boldsymbol{z}^I, \boldsymbol{z}^{II})$ at the grid star locations. This analogy xill come into play later, when errors due to unknown baseline orientation and length are analyzed.

3. ERROR ESTIMATES

The most important errors that enter the proposed calibration procedure the previous section are: *i)* baseline error, *ii)* star position error, and *iii)* measurement error (shot noise). Also, the truncation error of the finite-difference approximations of the derivatives of the calibration function and the error of the interpolation scheme for values of the calibration function between the grid stars must be added to these errors.

3.1. Error due to baseline error

The error in the estimate of the calibration function due to baseline error, e_b, arises from inaccuracies in the knowledge of the baseline vector, $\boldsymbol{b}$. Let us assume that the true baseline vector is given by $\boldsymbol{b} + \delta\boldsymbol{b}$ with

$$\delta\boldsymbol{b} \;=\; (\delta b_u,\, \delta b_v,\, \delta b_z)\,. \tag{32}$$

Then, according to (10)-(11), the error in the finite-difference approximation of the derivatives of the calibration function at the grid points is given by

$$\begin{bmatrix} \frac{1}{2\alpha} < \boldsymbol{s}, (R_v^+ - R_v^-)\delta\boldsymbol{b} > \\ \\ \frac{1}{2\beta} < \boldsymbol{s}, (R_u^+ - R_u^-)\delta\boldsymbol{b} > \end{bmatrix} = \begin{bmatrix} -\frac{\sin\alpha}{\alpha}(\gamma\,\delta b_u - u\,\delta b_z) \\ \\ -\frac{\sin\beta}{\beta}(\gamma\,\delta b_v - v\,\delta b_z) \end{bmatrix}. \tag{33}$$

To get estimates on the baseline error, assume that we have a regular, orthogonal grid, and let h denote the distance between any two adjacent stars. Then, according to (14)-(18) and (20), the baseline error at the grid stars satisfies the following overdetermined system

$$A \cdot e_b \;=\; 2h \begin{bmatrix} -\frac{\sin\alpha}{\alpha}(\gamma\,\delta b_u - u\,\delta b_z) \\ \\ -\frac{\sin\beta}{\beta}(\gamma\,\delta b_v - v\,\delta b_z) \end{bmatrix}. \tag{34}$$

The error e_b can be split into 3 parts, each one being a function of the baseline-vector error in one coordinate only, *i.e.*,

$$e_b = e_{bu}(\delta b_u) + e_{bv}(\delta b_v) + e_{bz}(\delta b_z) . \tag{35}$$

Then, relation (33) implies that

$$A \cdot e_{bu} = -2h \frac{\sin\alpha}{\alpha} \begin{bmatrix} \gamma \\ 0 \end{bmatrix} \delta b_u , \tag{36}$$

$$A \cdot e_{bv} = -2h \frac{\sin\beta}{\beta} \begin{bmatrix} 0 \\ \gamma \end{bmatrix} \delta b_v , \tag{37}$$

$$A \cdot e_{bz} = -2h \begin{bmatrix} u\frac{\sin\alpha}{\alpha} \\ \\ v\frac{\sin\beta}{\beta} \end{bmatrix} \delta b_z . \tag{38}$$

The individual components of the error e_b can be evaluated by solving the systems (34) through (36) in a least-squares sense, which amounts to multiplying both sides of these equations by $A^\dagger$. Each of the components of $\delta \boldsymbol{b}$ can be on the order of a micron. Therefore, the contribution of the baseline error to the calibration error is expected to be large.

It is important, however, to compare these errors to astrometric errors produced by innaccurate baseline knowledge. These "astrometric" baseline errors are of the form

$$< \boldsymbol{s}, \delta \boldsymbol{b}' > = u\delta b'_u + v\delta b'_v + z\delta b'_z ,$$

where $\delta \boldsymbol{b}' = (\delta b'_u, \delta b'_v, \delta b'_z)$ is the error in the baseline vector during the astrometric mesuarements. In other words, the "astrometric" baseline error is linear with respect to the grid coordinates, and its gradient is equal to the error in the baseline vector. Correction for this error is provided by the grid reduction procedure, [1], [2].

This implies that if the calibration error due to baseline-related error is also a linear, or approximately linear, function of the grid ccordinates, then it becomes *indistinguishable* from the astrometric error and will be corrected during the grid reduction. Therefore, we are only concerned with the *deviation* of this error from a linear function. In order to get estimates for this deviation we proceed with the following analysis.

Consider the first component of the baseline-related error in the calibration scheme, e_{bu}. This is the component that is associated with the stretch error in the baseline. The continuous analog to relation (36) is

$$\nabla e_b = -\frac{\sin\alpha}{\alpha} \delta b_u \, (\gamma \delta b_u, 0) . \tag{40}$$

By taking the divergence of this expression, we arrive at the following Poisson equation

$$\nabla^2 e_b = -\frac{\sin\alpha}{\alpha} \delta b_u \, \nabla \cdot (\gamma \delta b_u, 0) . \tag{41}$$

Employing the approximations $\sin\alpha \simeq \alpha$, and keeping the first two terms of the binomial expansion of γ (*i.e.*, $\gamma \simeq 1 - (u^2 + v^2)/2$), the above equation can be simplified to

$$\nabla^2 e_{bu} = u \, \delta b_u , \quad (u, v) \in D . \tag{42}$$

Dirichlet boundary data for this equation on a circular domain can be provided in the following manner. Now, consider a circle, T_R, of radius R equal to half the field of regard, and a unit vector $\boldsymbol{t}$ tangent to the circle. Then, we have

$$\begin{aligned} \nabla e_{bu} \cdot \boldsymbol{t} &= -\left(1 - \frac{u^2+v^2}{2}\right) \delta b_u \sin\theta\,, \quad (u,v) \in \partial T_R, \Rightarrow \\ \Rightarrow \nabla e_{bu} \cdot \boldsymbol{t} &= -\left(1 - \frac{R^2}{2}\right) \delta b_u \sin\theta\,, \quad (u,v) \in \partial T_R\,, \end{aligned} \tag{43}$$

where θ is the polar coordinate, $\theta = \arctan(v/u)$. Integrating the above relation along the perimeter of the circle T_R we obtain

$$\begin{aligned} e_{bu} &= -\left(1 - \frac{R^2}{2}\right) \delta b_u \int_0^\theta R \sin\phi \, d\phi \Rightarrow \\ \Rightarrow e_{bu} &= \left(R - \frac{R^3}{2}\right) (1 - \cos\theta)\, \delta b_u\,, \quad (u,v) \in \partial T_r\,. \end{aligned} \tag{44}$$

Let us now decompose the error component e_{bu} into to a term that is linear in u and a remaining term, in other words

$$e_{bu} = a_b u + \rho_u\,, \tag{45}$$

where a_b is a proportionality constant. The objective of the analysis is to compute an upper bound for the magnitude of ρ_u. According to this decomposition, the gradient of e_{bu} is given as

$$\nabla e_{bu} = (a_b, 0) + \nabla \rho_u\,. \tag{46}$$

Integrating this equation along the perimeter of the circle T_R we obtain an equivalent expression to (43),

$$\begin{aligned} e_{bu} &= R(\cos\theta - 1)\, a_b + \int_0^\theta \nabla \rho_u \cdot \boldsymbol{t}\, R\, d\phi\,, \quad (u,v) \in \partial T_r \Rightarrow \\ \Rightarrow e_{bu} &= R(\cos\theta - 1)\, a_b + \rho_u\,, \qquad (u,v) \in \partial T_r\,. \end{aligned} \tag{47}$$

Comparing (43) and (45), we observe that we can set

$$a_b = \delta b_u\,. \tag{48}$$

It is also worth mentioning that approximately the same solution for a_b is obtained by solving the discretized version of (41), with respect to e_{bu} and then passing a least-squares, linear fit through the solution. The discretized version of (41) is the overdetermined system (36) and has is solved in the least-squares sense.

Additionally, by inserting the ansatz (44) into (41), and by comparing (43) and (46), we finally arrive at the following boundary value problem for ρ_u on the circle T_R,

$$\nabla^2 \rho_u = u \delta b_u\,, \qquad (u,v) \in T_R\,, \tag{49}$$

$$\rho_u = (\cos\theta - 1)\, \frac{R^3}{2}\, \delta b_u\,, \quad (u,v) \in \partial T_r\,. \tag{50}$$

The solution to this problem can be written as a sum of two functions,

$$\rho_u = \rho_u^I + \rho_u^{II}\,, \tag{51}$$

where ρ_u^I is a nontrivial solution to the Poisson equation, and ρ_u^{II} is the solution to the Laplace equation with Dirichlet boundary data, i.e.,

$$\nabla^2 \rho_u^I = u\delta b_u \,, \qquad (u,v) \in T_r \,, \tag{52}$$

and

$$\nabla^2 \rho_u^{II} = 0 \,, \qquad (u,v) \in T_r \,, \tag{53}$$

$$\rho_u^{II} = -\rho_u^I(u,v) + (\cos\theta - 1)\frac{R^3}{2}\,\delta b_u \,, \quad (u,v) \in \partial T_r \,. \tag{54}$$

A nontrivial solution to (51) is readily found to be

$$\rho_u^I = \frac{1}{8} r^3 \cos\theta\, \delta b_u \,, \tag{55}$$

which implies that

$$|\rho_u^I| \leq \frac{\delta b_u}{8} R^3 \,. \tag{56}$$

Subsequently, inserting (55) into the boundary condition (54) yields

$$\rho_u^{II} = (\frac{3}{8}\cos\theta - \frac{1}{2})R^3\,\delta b_u \,, \quad (u,v) \in \partial T_R \,. \tag{57}$$

An upper bound for $|\rho_u^{II}|$ is directly obtained by virtue of the maximum principle for the Laplace equation,

$$|\rho_u^{II}| \leq \frac{7}{8} R^3\,\delta b_u \,. \tag{58}$$

Combining relations (50), (55), and (57) we finally get

$$|\rho_u| \leq R^3\,\delta b_u \,. \tag{59}$$

This expression provides and upper bound for the deviation of the first component of the baseline error e_{bu} from a linear function.

A similar result holds for the second component of the baseline error, e_{bv}. The continuous analog of (37) is

$$\nabla^2 e_{bv} = v\,\delta b_v \,, \quad (u,v) \in D \,. \tag{60}$$

Setting $e_{bv} = v\delta b_v + \rho_v$ and performing the same analysis as above for ρ_v, we find that the same upper bound holds for ρ_v, *i.e.*,

$$|\rho_v| \leq R^3\,\delta b_u \,. \tag{61}$$

For the third component, e_{bz}, we have the continuous analog to (38)

$$\nabla e_{bz} = -(u,v)\,\delta b_z \,, \quad (u,v) \in D \,, \tag{62}$$

where the approximations for $\sin\alpha \simeq \alpha$ and $\sin\beta \simeq \beta$ have been employed. As usual, e_{bz} is decomposed into a term which is linear with respect to γ and a remainder,

$$e_{bz} = \gamma\delta b_z + \rho_z \simeq (1 - \frac{u^2+v^2}{2})\delta b_z + \rho_z \,. \tag{63}$$

Taking the gradient of this expression and comparing it with (62) we arrive at

$$\nabla \rho_z = 0 \,, \quad (u,v) \in D \,, \tag{64}$$

which means that ρ_z is a constant function and, therefore, it can be solved as part of the grid reduction. This result, combined with (56) and (58) suggests that the deviation of the baseline error from a linear function of the form $u\delta b_u + v\delta b_v + \gamma\delta b_z$ is bounded by the term $R^3(\delta b_u + \delta b_v)$.

3.2. Error due to measurement noise

Let $\eta_{u_i}^{\pm}$, and $\eta_{v_i}^{\pm}$, $i = 1, \ldots, N^2$, be the variables representing the noise in each delay measurement $d_{u_i}^{\pm}$ and $d_{v_i}^{\pm}$, respectively, at the grid stars. Let us assume for simplicity that we have a regular grid. As before, let h denote the distance between any two adjacent stars. Noise enters (20) via

$$A\hat{c} = \boldsymbol{z} + \frac{h}{\alpha}\boldsymbol{\eta}, \tag{65}$$

where $\boldsymbol{\eta} = [\boldsymbol{\eta}_u, \boldsymbol{\eta}_v]^{\mathrm{T}}$, $\boldsymbol{\eta}_u$ and $\boldsymbol{\eta}_v$ being random N^2-vector with components η_{ui} and η_{vi}, respectively. Further, we have $E(\eta_{u_i}^2) = 2E([\eta_{u_i}^{\pm}]^2)$ and $E(\eta_{v_i}^2) = 2E([\eta_{v_i}^{\pm}]^2)$. Henceforth we will write σ_η for the single measurement error, *i.e.*, $E(\eta_{u_i}^2) = E(\eta_{v_i}^2) = 2\sigma_\eta^2$.

Now let $Y = A^{\mathrm{T}}A$. Further, let λ_k, $k = 1, \ldots, N^2$, denote the eigenvalues of Y. Then, the variance to the solution of (64) is related to the sum of the reciprocals of the nonzero eigenvalues, *viz*

$$E(|c - \hat{c}|^2) = \frac{2\sigma_\eta^2 h^2}{\alpha^2} \sum_{\lambda_k \neq 0} \frac{1}{\lambda_k}. \tag{66}$$

Therefore, the rms error due to measurement noise is

$$\sqrt{\frac{E(|c - \hat{c}|^2)}{N^2}} = \frac{\sigma_\eta}{N}\frac{h}{\alpha}\sqrt{2\sum_{\lambda_k \neq 0}\frac{1}{\lambda_k}}. \tag{67}$$

It is quite difficult to obtain an analytic expression for the sum of the eigenvalues that appears in the above relation. However, it can be shown that the eigenvalues of this matrix are larger than the expressions $4 - 2\cos(\pi i/N) - 2\cos(\pi j/N)$, $i, j = 1, \ldots, N$. The sum of the reciprocals of these expressions are $O(N^2 \log N)$. Therefore, it is meaningful to try to approximate this sum by a function of the form $aN^2 \log N$, with a being a constant coefficient, for the sum of the reciprocals of the eigenvalues. One can indeed verify that for N in the range of interest, $8 \leq N \leq 25$, the following approximation holds

$$\sum_{\lambda_k \neq 0} \frac{1}{\lambda_k} \simeq \left(\frac{N}{6} - 1\right) N \log N, \tag{68}$$

which, in view of (66), implies that the rms error due to measurement noise satisfies

$$\sqrt{\frac{E(|c - \hat{c}|^2)}{N^2}} < \sigma_\eta \frac{h}{\alpha}\frac{\sqrt{\log N}}{\sqrt{3}}. \tag{69}$$

If $h = \alpha$, then the rms error due to measurement noise will be smaller than the rms of the noise if $N \leq 20$.

Note also that noise propagation decreases linearly with the magnitude of the roll/cant angle and sublinearly with increasing the number of stars in the grid, since h $1/N$. The problem with increasing the roll/cant angle is that a greater discretization error results. The diffuculty with increasing the number of stars in the grid is the time to perform the calibration (the required time is proportional to N^2).

3.3. Error due to star position error

The motivation for performing the calibration procedure as differential measurements was to reduce the sensitivity to errors in the knowledge of star position. These are vectors of the form

$$\delta \boldsymbol{s}_i = \left(h_{ui},\, h_{vi},\, -\frac{u_i h_{ui} + v_i h_{vi}}{\gamma_i}\right), \quad i = 1, \ldots, N^2. \tag{70}$$

These errors enter (18) via

$$A\hat{c} = z + \frac{h}{\alpha}\eta_s, \tag{71}$$

where η_s is a $2N^2$-vector that represents the error in the difference operators of the calibration function due to the star position errors. According to (10) and (11) η_s has the following form

$$\eta_s = \begin{bmatrix} < \delta s, (R_v^+ - R_v^-)\, b \\ < \delta s, (R_u^+ - R_u^-)\, b \end{bmatrix}, \tag{72}$$

which, in view of (3) and (5), becomes

$$\eta_s = -2|b| \sin\alpha \begin{bmatrix} (uh_u + vh_v)/\gamma \\ 0 \end{bmatrix}. \tag{73}$$

Here h_{ui} and h_{vi}, $i = 1, \ldots, N^2$, are zero-mean uncorrelated random variables with $E(h_{ui}^2) = E(h_{vi}^2) = \sigma_s^2/2$, σ_s being the rms position error of a grid star in one coordinate direction.

Relation (69) implies that the star position errors have no effect at all to the approximations of the v-derivatives of the calibration function. Therefore, in order to get an estimate for the rms error due to star position error, let $Y_u = A_u^T A_u$, and let λ_u denote the eigenvalues of Y_u. The variance of the solution to (67) is related to the reciprocals of the non-zero eigenvalues, and an upper bound is given by

$$E(|c - \hat{c}|^2) < \frac{(2|b|h\sigma_s \sin a)^2}{2\alpha^2} 2\left(\frac{N}{2}h\right)^2 \sum_{\lambda_{uk}\neq 0} \frac{1}{\lambda_{uk}} \simeq (N|b|h^2\sigma_s)^2 \sum_{\lambda_{uk}\neq 0} \frac{1}{\lambda_{uk}}. \tag{74}$$

From this expression, the following bound for the rms error due to star position error is derived:

$$\sqrt{\frac{E(|c - \hat{c}|^2)}{N^2}} < |b|\, h^2\, \sigma_s \sqrt{\sum_{\lambda_{uk}\neq 0} \frac{1}{\lambda_{uk}}}. \tag{75}$$

As before, the sum appearing in the above relation can not be evaluated in closed form. However, it can be easily computed numerically. Furthermore, a good approximation for this sum is given by the following relationship

$$\sum_{\lambda_{uk}\neq 0} \frac{1}{\lambda_{uk}} \simeq \frac{1}{12} N^3 - 3N. \tag{76}$$

It turns out that for N within the range of interest, $10 \leq N \leq 20$, the rms error is much smaller than $|b|\,\sigma_s$. For example, if $N = 16$ and $h = 1°$ (implying that the field of regard is 15°), then the rms error is smaller than 5% of $|b|\,\sigma_s$.

3.4. On the truncation and interpolation errors

The proposed calibration scheme is based on constructing centered-difference approximations of the first-order derivatives of the calibration function. It is well known from standard numerical analysis that, on a uniform grid, the higher-order term of the error, e_t of the approximation of the u-derivative is given by

$$e_t = \frac{h^2}{6}\frac{\partial^3 c}{\partial u^3} + \text{h.o.t.}, \tag{77}$$

where h is the distance between two adjacent grid points. A similar expression holds for the v-derivative.

Interpolation of the calibration function at arbitrary points inside the field of regard introduces errors that can also be expressed in terms of the high-order derivatives of c. For example, for linear 1D interpolation along the u direction (interpolation along a line segment) the error is given by

$$e_i = \frac{(h - \Delta u)\,\Delta u}{2}\,\frac{\partial^2 c}{\partial u^2} + \text{h.o.t.}\,, \tag{78}$$

where $\Delta u < h$ is the distance between the point of interest and the location of the adjacent grid star from the left side.

These results, however, do *not* necessarily suggest that we have to be concerned with the high-order derivatives of the calibration function that we are trying to estimate. The reason is that our objective is not to determine the *true* calibration function c but an *admissible* calibration function, say $\tilde{c}$, which satisfies

$$\|c - \tilde{c}\|_\infty \;\leq\; e_c\,, \tag{79}$$

where $\|\cdot\|_\infty$ denotes the maximum norm, and e_c is a small allowable tolerance, whos precise value is to be determined. For example, it is meaningless to set e_c to a value smaller than the size of the errors due to measurement noise. Any function $\tilde{c}$ is admissible as long as it satisfies (79) which implies that it is sufficient to try to estimate $\tilde{c}$ instead of c. The smoothness of $\tilde{c}$ will be detrmined via testing, modeling, and analysis. The exact procedure for this has not yet been defined.

If, for example, $\tilde{c}$ is a third-order polynomial then the effects of the interpolation and trunction errors can be easily written in terms of the polynomial's coefficients. Indications on the form and smoothness of admissible calibration functions will be provided by ground experiments and computational modeling of the physical phenomena that are affect delay measurements, such as diffraction, polarization effects *etc.* The existing numerical evidence on the effects of these phenomena indicates that 3rd-order polynomials can indeed be admissible calibration functions.

4. NUMERICAL RESULTS

The proposed external calibration algorithm was tested on a series of numerical tests that are described below. We considered a grid of 16×16 stars, covering a $15° \times 15°$ field of regard, *i.e.*, $N = 16$ and $h = 1°$. These are typical values, given the mission requirements for SIM and the 'density' of bright stars (magnitude 11 and above) at any portion of the sky. Actually, it is anticipated that N may be as low as 10, but not higher than 20.

It was assumed that the shot noise of the instrument follows a Gaussian distribution of zero mean and variance $\sigma_\eta = 250\ pm$. Further, it was assumed that the star position error is also a Gaussian distribution of zero mean and variance $\sigma_s = 10^{-8}\ rads \simeq 2 \times 10^{-3}\ arcsec$. To measure the effect of these random errors, approximately 20 Monte Carlo simulations were ran and the rms error in the calibration function was computed. The range of the rms error from each set of Monte Carlo simulations is given below. Finally, the baseline vector was assumed to be $\boldsymbol{b} = (10, 0, 0)\ m$, while the error of the baseline vector was taken to be $1\ \mu m$ on each component.

The "true" calibration function was derived from estimates of the polarization and diffraction effects on the metrology systems. It is a 2nd order polynomial on u and v plus a small-amplitude sinusoidal perturbation on each direction. A plot of this function along the v-axis is given below, Fig. 1.

In the **first test**, a uniform grid was considered. Assuming zero errors from baseline, star position and measurement noise, the error on the estimation of the calibration function was $32pm$. This error arises from the truncation of the derivatives and represents the lower bound of the overall error of the proposed

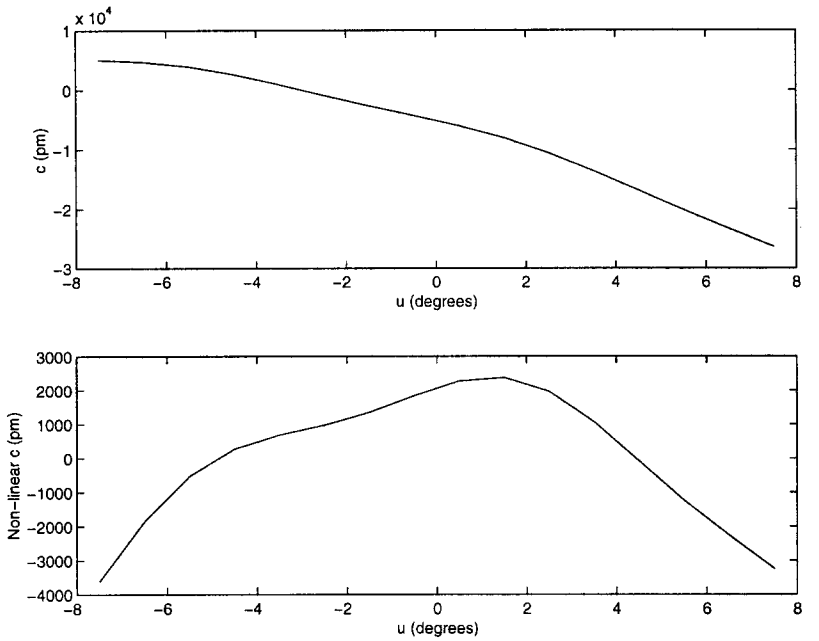

Figure 1. Top: plot of the "true" calibration function, c, along the v-axis. Bottom: Plot of the nonlinear part of c.

scheme. When a lower resolution grid was employed, consisting of 11×11 stars, this error increased to 139 pm.

When we took into account the effect of measurement noise only and ran 20 Monte Carlo simulations, the rms error varied between $186 - 269$ pm. Similarly, when we examined the effect of the star-position error, the rms error on the calibration function varied between $132 - 228$ pm. Finally, when we considered the combined effect of shot noise, star-position and baseline-vector errors, the residual rms error in the calibration function lied between $249 - 401$ pm. This residual error does not include the linear part of the baseline-vector error because it can be evaluated as part of the grid reduction. Plots of the true and estimated calibration functions (for one particualr numerical test) are shown if Fig. 2.

In the **second test**, we generated irregular grids by assuming randomly distributed stars across the field of regard, with a density of 8 stars per square degree (this is a realistic density value of stars that satisfy brightness and size requirements). During each numerical experiment, the stars that were closest to the grid points of the corresponding regular grid were selected as the grid stars. A plot of one grid realization is given in Fig. 3. As in the first test, sets of 20 Monte Carlo simulations were conducted to examine the effect of the various errors. For these simulations, random realizations for both the stochastic errors (star-position error and shot noise) and the star-grid were eployed. In the presence of discretization error only, the standard deviation of the error in the calibration function lied between $61 - 81$ pm. In other words, there was an increase on the order of $30 - 50$ pm in the discretization error due to the irregularity of the grid. Assuming noise in the measurements (and absence of star-position and baseline errors), the rms calibration error was between $201 - 254$ pm, which implies a 10 pm increase from the regular-grid case. Similarly, assuming star position error (and absence of measurement noise and baseline errors), the rms. calibration error was found to be between $137 - 208$ pm.

When all posible errors were taken into account, the rms. error was between $260 - 320$ pm, *i.e.*, at the same levels as in the first test. The plots of the true calibration function and the estimated one (for one particular numerical test) are shown in Fig. 4. The difference between the true values and the numerically computed

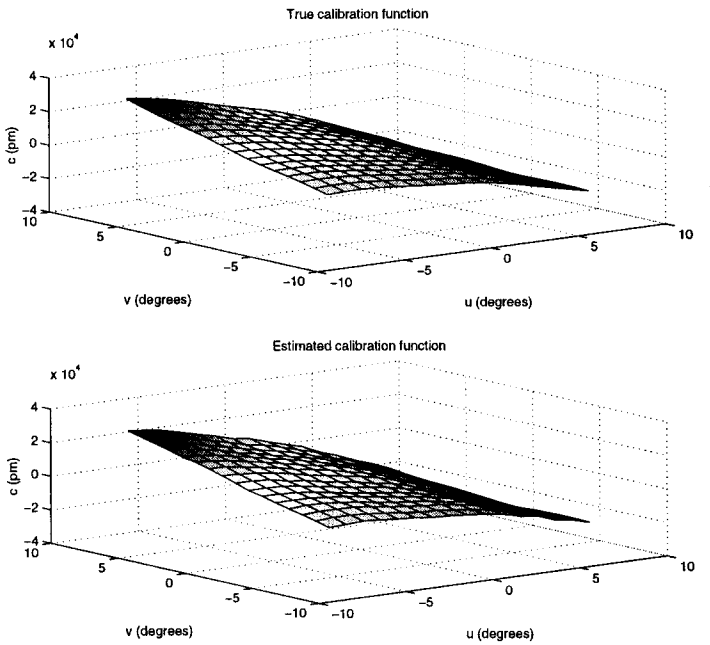

Figure 2. First test, regular grid. True and estimated calibration function, on a $15° \times 15°$ field of regard.

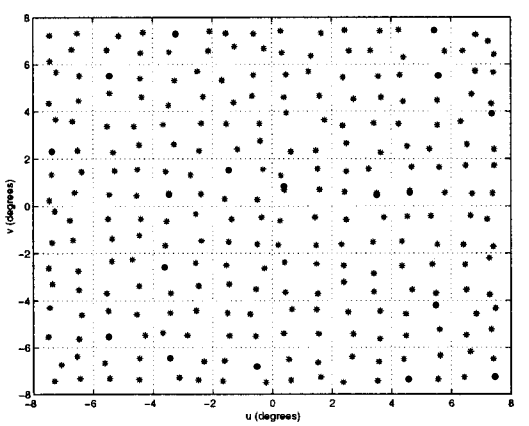

Figure 3. Second test. Irregular grid of one Monte Carlo simulations. The stars were picked among 1800 stars randomly distributed across the field of regard (star density, 8 stars per square angle.

ones are shown in Fig. 5. As before, the linear part of the baseline-vector error has been subtracted from these results. A plot of the linear part correction is shown in Fig. 6.

For the **third test**, the a grid based on the "self-start" scenario of SIM was constructed. In particular, we considered a 10×10 grid on a $15°$ field of regard with a priori star-position error of approximately 20 *mas*. Subsequently, new star positions were estimated via simulation of the measurement process of SIM. These simulations reduced the star-position error to approximately 2 *mas*. It should be noted, however, that since the new grid-star locations were computed by means of an estimation procedure, the errors are now correlated, in contrast to the previous two tests where the star-position errors were uncorrelated. The numerical results are summarized in the next paragraph. The numbers inside parentheses that follow the results below are the equivalent results for randomly generated 10×10 grids on $15°$ field of regard (in other words, for the results inside parentheses a new generalization for the star grid was used for each Monet Carlo simulation).

The dicretization error was found to be 162 *pm*, (153 – 188 *pm*). The rms error in the presence of

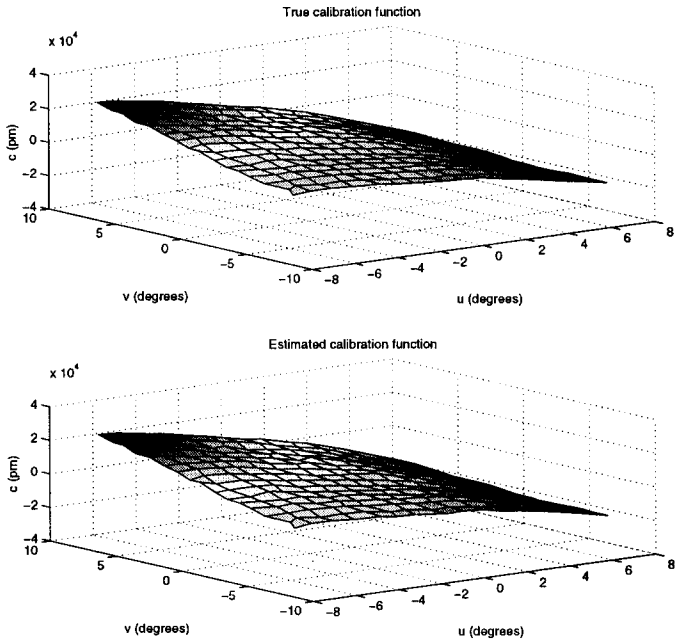

Figure 4. Second test, irregular grid. True and estimated calibration function, on a $15° \times 15°$ field of regard.

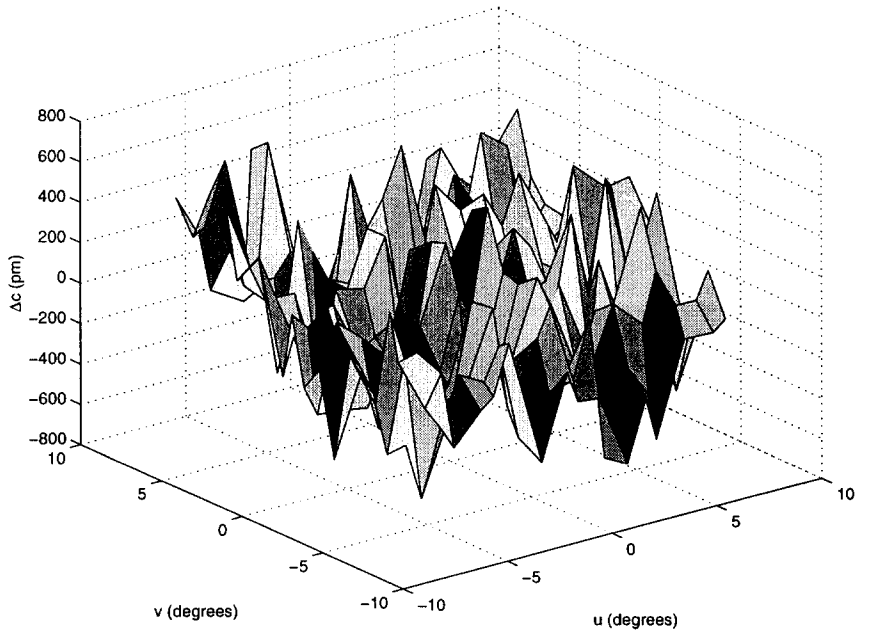

Figure 5. Second test, irregular grid. Difference between true and estimated calibration function, Δc, across the $15° \times 15°$ field of regard.

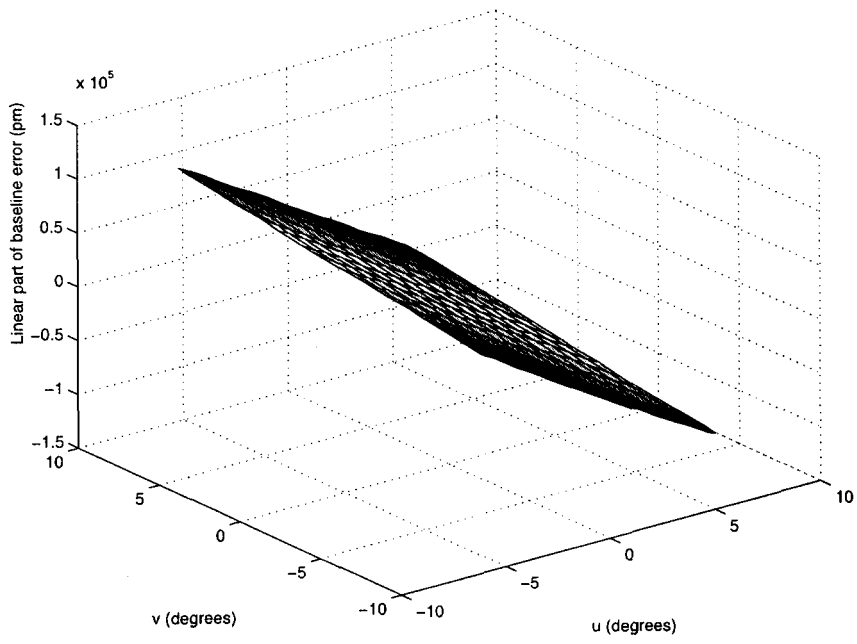

Figure 6. Second test, irregular grid. The linear part of the calibration-vector error. This part will be solved as part of grid reduction.

Type of Error	Root Mean Square error (pm)		
	1st Test	2nd Test	3rd Test
Discretization Error	32	61 – 81	162 (153-188)
Measurement Noise	186 – 269	201 – 254	330 – 444 (318-544)
Star-position error	132 – 228	137 – 208	275 – 598 (213-473)
All errors	249 – 401	260 – 320	418 – 653 (379-550)

Table 1. Summary of results of the 3 tests.

measurement noise was $330 - 444$ pm, ($318 - 544$ pm). The rms error in the presence of star-position error was between $375 - 598$ pm ($255 - 381$ pm). Finally, the combined effect of all errors generated rms errors of $418 - 653$ pm, ($379 - 550$ pm). The overall errors from this "self-start" scenario are generally higher than those resulting from randomly generated grids because the individual error components become correlated.

These results indicate that in order to keep the overall error below 0.5 nm, a resolution of 1 star per degree angle along each direction is necessary. It should be mentioned that these results could have been different if a different calibration function had been assumed. At the present time we do not know exactly the form of the calibration function that we should expect. However, as mentioned above, ground experimental data and numerical simulations will provide indications about the form of the function. Then it would be possible to derive firm resolution requirements and more accurate error bounds. The results of the tests that were carried taken during the present study are summarized in the following table.

5. CONCLUDING REMARKS

A procedure for external calibration of SIM was presented. The objective of external calibration is to determine a calibration function that corrects field dependent errors in the delay measurements made by the instrument. This procedure consists of the following steps.

The first step is to set up a grid of stars within the instrument's field of regard. Then, finite-difference approximations of the derivatives of the calibration function are constructed from direct measurements on the grid stars by rotating the baseline of the instrument. This procedure results in an overdetermined linear system with respect to the values of the calibration function at the field points corresponding to the grid star locations. This system is then solved in the least-squares sense. Interpolation between the computed values produce values of the calibration function at any point within the field of regard.

Analytic or semi-analytic bounds for the errors generated by the proposed procedure have been derived. These bounds indicate that, given the various design parameters of SIM, the procedure has the potential of being sufficiently accurate and robust. The timescale for implementing the calibration procedure appears to be within reasonable bounds for wide angle mission requirements.

The efficacy of the procedure was demonstrated through a series of tests. In particular the effect of each error was studied through Monte-Carlo simulations. The discretization error was found to be on the order of 50 pm for sufficiently dense girds (approximately 15×15 stars), while measurement noise contributes rms errors on the order of 250 pm. Seperately, the star-position error, created rms errors of approximately 150 pm. When all errors were taken into account, it was found that it is possible to expect rms errors around or below $0,5$ nm. This implies that the analytically derived error bounds are conservative with respect to the numerical results. Near term work will focus on meshing the procedure and error analysis with testbed and modeling developments and requirements.

ACKNOWLEDGMENTS

This work was prepared at the Jet Propulsion Laboratory, California Institute of Technology, under a contract with National Aeronautics and Space Administration.

REFERENCES

[] Milman, M.H., "A note on SIM external calibration feasibility," *JPL Interoffice Memorandum*, July 2000.

[] Milman, M.H., "Miscellaneous musings about the measurements made by SIM," *JPL Interoffice Memorandum*, September 2000.

[] Catanzarite, J., & Milman, M.H., "Accuracy requirements on baseline orientation and star positions," *JPL Interoffice Memorandum*, October 2000.